Head-Direction Cells in Postsubiculum Show Systematic Parallax Errors During Visual Anchoring

Sven Krausse
Forschungszentrum Jülich - PGI 15
RWTH Aachen University - Institute for Electrical Engineering and Information Technology
Aachen, Germany
s.krausse@fz-juelich.de

Emre Neftci
Forschungszentrum Jülich - PGI 15
RWTH Aachen University - Institute for Electrical Engineering and Information Technology
Aachen, Germany

Friedrich T. Sommer
UC Berkeley - Redwood Center for Theoretical Neuroscience
Berkeley, USA

Alpha Renner
Forschungszentrum Jülich - PGI 15
Aachen, Germany
a.renner@fz-juelich.de

Abstract

Spatial navigation relies on the head-direction (HD) system, which integrates angular head velocity (AHV) to track orientation. Since integration accumulates drift over time, visual landmarks provide corrective cues. However, whether the HD system explicitly accounts for the apparent shift in proximal objects' position when viewed from different angles remains unclear. These shifts are caused by the parallax effect, where closer objects move more strongly on the retina than distant ones.

Here, we analyzed postsubicular HD cell activity in mice navigating with a single visual cue. We discovered a systematic parallax bias in the decoded HD, indicating that the HD system misinterprets the cue's position depending on the viewing angle. The observed error was smaller than predicted by a pure vision model, which can be explained by the combination of AHV integration with simple visual anchoring.

Notably, each animal exhibited a unique anchoring angle — the direction at which the cue was associated with head direction — suggesting that the HD system maintains a relatively stable and possibly learned mapping between the cue angle from visual input (bearing) and head direction.

These results provide evidence that the HD system, at least in simplified environments, does not perform explicit parallax correction but may instead attenuate errors passively through AHV integration and simple anchoring to multiple cues. This highlights a fundamental trade-off in neural coding between computational efficiency and positional accuracy, with implications for biological and artificial navigation systems.

Keywords: navigation; postsubiculum; parallax; sensory integration; head-direction cells; bearing cells; landmark anchoring

Introduction

Accurate spatial navigation depends on a reliable sense of direction, which is mediated by the head-direction (HD) cell network. HD cells, discovered in many brain areas including postsubiculum (Rank, 1984), thalamus (Taube et al., 1990a), lateral mammillary nucleus (Stackman & Taube, 1998), and entorhinal cortex (Giocomo et al., 2014), encode the animal's orientation in allocentric coordinates, effectively serving as an internal neural compass. These cells are tuned to specific head directions, collectively forming a continuous representation of orientation. HD cells receive input from angular head velocity (AHV) cells, which signal changes in head direction (computed from vestibular inertial, proprioceptive, and optic flow signals) and enable the HD network to integrate angular velocity over time (McNaughton et al., 1991, 2006). This integration process, often modeled as a 1D continuous (ring) attractor network (CAN) (Skaggs et al., 1994; Zhang, 1996; Redish et al., 1996; Chaudhuri et al., 2019), provides a persistent representation of head direction. However, integration alone is prone to accumulating noise, which necessitates periodic recalibration through external sensory inputs such as visual landmarks.

Visual landmark cues play a crucial role in anchoring the HD system to stable reference points in the environment (Taube et al., 1990b; Goodridge et al., 1998; Knierim et al., 1995; Zugaro, Berthoz, & Wiener, 2001). Empirical studies have demonstrated that HD cells align their preferred firing direction (PFD) with distal visual landmarks (Taube et al., 1990b). When a cue is rotated, the PFD of HD cells shifts

accordingly, indicating that external visual information recalibrates the internal representation of head direction (Taube et al., 1990b). Simulations and ablation studies support the essential role of HD cells in robust spatial navigation. As sketched in Fig. 1, HD cells in the postsubiculum (PoSub) receive inputs originating from visual cortex, the vestibular system and proprioception (Blair & Sharp, 1996; Goodridge et al., 1998; Knierim et al., 1995; Zugaro, Berthoz, & Wiener, 2001; Hulse & Jayaraman, 2020), and PoSub relays landmark anchoring back to the lateral mammillary nuclei (Yoder et al., 2015) and head direction forward to entorhinal cortex; disrupting the HD cell network impairs parahippocampal grid cell activity and degrades path integration (Winter et al., 2015; Wilton et al., 2001; Butler et al., 2017). Additionally, bearing cells were found in the retrosplenial cortex, encoding the egocentric distance and angle of landmarks in the environment and projecting to PoSub (Alexander et al., 2020).

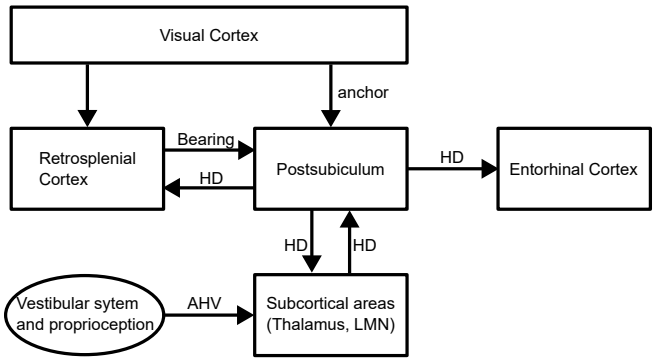

Figure 1: **Illustration of functional connectivity in the HD circuit after Hulse & Jayaraman (2020); Taube (2007)**.

Despite the established role of visual cues in HD anchoring, open questions remain. For instance, it is not entirely clear whether visual inputs correct HD representations in a simple, cue-anchored manner based on the location of the cue on the retina (corrected by the eye's current pose) or through complex computations that involve relative positional information to remove the position-dependent error arising from parallax, particularly for proximal cues. Parallax is the apparent shift in an object's position when viewed from different angles, where closer objects seem to move more strongly on the retina than distant ones. Previous research shows that distal cues (which suffer less from parallax) have a stronger influence on HD anchoring than proximal ones (Zugaro, Berthoz, & Wiener, 2001; Knierim & Hamilton, 2011). Models postulate a parallax error under the assumption of simple visual anchoring (Bicanski & Burgess, 2016) and came up with solutions on how to avoid parallax (Bicanski & Burgess, 2016; Page & Jeffery, 2018; Stratton et al., 2010). However, to our knowledge, the HD system has not been shown to exhibit systematic parallax-induced error.

In this study, we analyze recordings of postsubicular head direction cells of mice navigating a circular platform with a single visual cue. As we find a systematic HD error that can be explained by parallax, we favor the idea that the HD network primarily uses simple cue anchoring rather than complex computations involving relative positional information. The error mouse HD cells made in our analysis is only about half as large as the expected parallax error. We demonstrate that attenuation can occur passively through AHV integration and visual anchoring at different locations, averaging out parallax errors. In richer environments, the availability of multiple visual cues can eliminate parallax errors thanks to simple averaging (Gaussier et al., 2019) and enhance the stability of the HD representation. However, this study does not rule out the possibility that under richer environmental conditions, where multiple distal and proximal cues are present, the HD system may employ additional correction mechanisms beyond simple averaging. The extent to which these mechanisms operate remains an open question.

Together, these findings provide new insights into how visual input anchors vestibular AHV integration in HD computation.

Methods and Results

Experimental Data and Environment

We analyzed publicly available neural recordings from the postsubiculum (PoSub) of six mice during the "Cue Rotation Task" from Dataset 3 (Duszkiewicz et al., 2024). This dataset includes tracked head position and direction and spike trains. Mice freely explored a 30 cm diameter elevated circular arena within a 90 cm darkened square enclosure (Fig. 2A) for approximately 75 minutes per session. Visual cues, consisting of dim LED strips forming a "V" or "X" shape (approximately 10 cm wide), were positioned at the center of each wall and treated as point sources for analysis. Surgical procedures, electrophysiological recording details, and the exact experimental protocol are described in (Duszkiewicz et al., 2024).

Each session began with a stable cue presentation (15-20 minutes). Subsequently, this initial cue was turned off, and a cue on an adjacent wall was activated. Only one cue was active at any time. The experimental protocol comprised 16 200-second trials, with the active cue alternating between the two LEDs after each trial.

Data Exclusion

For the decoding error, we assume that the allocentric reference frame rotates with the cue (effectively removing the cue switches), which is in line with the behavior of the HD system. We rejected data right after cue switches (except for the optimization of the σ in Eq. 8) as the decoding error took a variable amount of time to decrease. To avoid the exclusion of a too large amount of data, we fitted an exponential function with a delay to the head direction decoding error signal to determine the switching timepoint and excluded the data between trial onset and one second after that point. Additionally, 3 trials in which the HD system did not respond to the cue switching were manually excluded. We also excluded periods where the mice exhibited prolonged immobility (no angular head velocity

for more than 5 seconds), as these periods often had reduced overall spiking activity and therefore increased decoding uncertainty. Three intervals of 50-300s with large decoding errors were manually excluded.

Additionally, we implemented tracking error detection to reject the few time intervals with unreliable head direction tracking. These periods were identified by computing the difference between the tracked head direction and its low-pass filtered version (5-second sliding window average). We removed instances of implausibly large head direction jumps ($> 2000^\circ/s$). Smaller jumps for only a few bins were imputed by linear interpolation.

HD Decoding

As Duszkiewicz et al. (2024), we performed Bayesian decoding (Zhang et al., 1998) on the head direction cells (cell labeling adopted from the dataset). Tuning curves for all head direction neurons were computed using the initial 15-20 minutes of each session before the first trial. This period was excluded from subsequent analysis. The Bayesian decoder treats these tuning curves as conditional probability distributions of head direction given a neuron's firing. For each time bin of 10 ms, the likelihood distribution of the head direction was calculated by multiplying the tuning curves of all spiking neurons within that bin. The prior is the head direction distribution of the preceding time bin and discourages large jumps between consecutive estimates. The head direction estimate for each time bin was then obtained by identifying the peak of the resulting posterior. Notably, the number of HD neurons per dataset varied between 46 neurons (Mouse 5) and 104 neurons (Mouse 4), leading to a difference in decoding quality (see Suppl. Fig. 11).

α_{true}	'true' HD extracted from tracking data
α_{dec}	HD decoded from neural data
α_{vis}	HD from pure vision cue anchoring
α_{iv}	HD from the integrate-and-vision model
$\Delta\alpha$	Angular displacement between timesteps
θ_{cue}	Allocentric angle of the vector from the animal to the cue
ϕ_{cue}	Bearing angle: Egocentric angle of the cue (from the animal's perspective)
γ_{anchor}	Anchoring angle of the cue, mapping bearing to HD representation
β_{dec}	Decoding error of decoded neural HD signal
β_{vis}	Error of the vision-based HD signal (parallax-error)
Δx	Lateral offset of the animals position relative to the cue
Δy	Longitudinal offset of the animals position relative to the cue
σ	Weighting parameter in integrate-and-vision model

Table 1: Reference for variables and nomenclature.

Computation of Vision-Based Head Direction

Here, we want to understand what the animal sees at each point in time during its walk on the platform and estimate the head direction (HD) based purely on the visual cue, independent of the neural data.

First, we computed the egocentric angle of the cue relative to the animal's position at each step. Given the lateral and longitudinal offsets, Δx and Δy, of the animal from the cue (Fig. 2B), the allocentric cue angle θ_{cue} is defined as:

$$\theta_{\text{cue}}(t) = \arctan\left(\frac{\Delta y(t)}{\Delta x(t)}\right). \tag{1}$$

Importantly, θ_{cue} is independent of the HD of the animal and only depends on its position on the platform.

The perceived cue angle (egocentric angle) ϕ_{cue} corresponds to the retinal location of the cue, corrected by the current eye angle. Here, we can compute it directly as the angular difference between the true head direction α_{true} (from head tracking) and θ_{cue}:

$$\phi_{\text{cue}}(t) = \alpha_{\text{true}}(t) - \theta_{\text{cue}}(t). \tag{2}$$

For readability, we omit the wrapping of angles from the equations. In practice, whenever we take sums or differences of angular measurements, we apply a wrapping function $f(x) = \arg(e^{ix})$ to the result of the addition/subtraction.

This signal corresponds to the activity of bearing cells, which encode relative object angles (e.g., $\phi_{\text{cue}} = 0^\circ$ when the cue is directly ahead, $\phi_{\text{cue}} = 90^\circ$ when it is to the left). In our analysis, we assumed a fixed association between ϕ_{cue} and an internal head direction estimate.

To model a simple visual anchoring mechanism, we defined the vision-based HD estimate α_{vis} using a fixed anchoring direction γ_{anchor}, that could, for instance, have been learned or is determined by cue features:

$$\alpha_{\text{vis}}(t) = \gamma_{\text{anchor}} + \phi_{\text{cue}}(t). \tag{3}$$

This formulation assumes that the HD system aligns its preferred firing direction with the egocentric angle of the cue without correcting for positional changes due to parallax. The implications of this assumption are explored in the following sections.

Parallax-Induced Head Direction Error

If the HD system strictly followed an egocentric anchoring mechanism (head direction is cue direction ϕ_{cue} plus a fixed offset γ_{anchor}, see Eq. 3), then parallax should introduce systematic errors in the estimated HD. We define the parallax-induced error $\beta_{\text{vis}}(t)$ as the angular difference between the vision-based HD estimate α_{vis} and the 'true' HD α_{true} from the tracking system:

$$\beta_{\text{vis}}(t) = \alpha_{\text{vis}}(t) - \alpha_{\text{true}}(t). \tag{4}$$

Substituting α_{vis} with the expressions from Eqs. 1, 2, and 3 lets us express the error of the vision model as a function

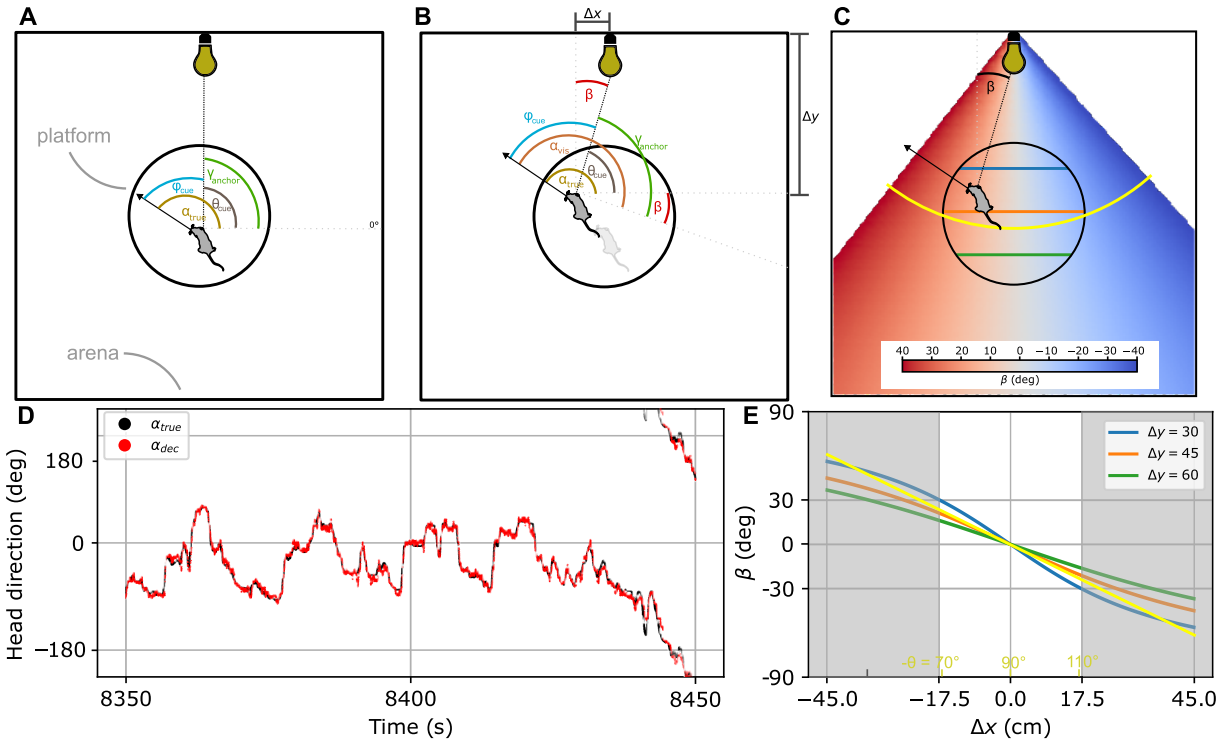

Figure 2: **Illustration of position-dependent parallax error in head direction (HD) estimation.** (**A**) Schematic of the experimental setup: the animal navigates a circular platform with a single visual cue positioned at the north wall. Angles needed in the equations of this paper and listed in Table 1 are charted. (**B**) The parallax effect: when the animal moves laterally while maintaining the same true head direction, the relative angle to the egocentric angle changes, introducing a systematic bias β in the visually anchored HD estimate. (**C**) Parallax-induced error β color-coded at different locations in the arena, based on Eq. 5. The four colored lines through the arena are the trajectories along which the error is plotted in panel E. (**D**) Arbitrary example data from Duszkiewicz et al. (2024) showing the true head direction and the decoded head direction. The difference between these two curves β_{dec} is used for the linear regression in Eq. 7. (**E**) Parallax-induced error β as a function of lateral displacement Δx for three different distances Δy from the cue. Distances are also shown in panel C. The error is not linearly dependent on $\Delta x(t)$ but rather on $\theta_{\text{cue}}(t)$ (yellow line). We, therefore, perform the linear regression using this angle.

of the angle between the animal and the cue or lateral and longitudinal offsets:

$$\begin{aligned}\beta_{\text{vis}}(t) &= \gamma_{\text{anchor}} - \theta_{\text{cue}}(t) \\ &= \gamma_{\text{anchor}} - \arctan\left(\frac{\Delta y(t)}{\Delta x(t)}\right).\end{aligned} \tag{5}$$

This formulation predicts a systematic relationship between β and the animal's position, induced by parallax, visualized in Fig. 2C,E. The error is linear with respect to $\theta_{\text{cue}}(t)$, as shown in Fig. 2E.

To test whether such a systematic error is also visible in the recorded neural data, we compute the decoding error of the head direction β_{dec} as the angular difference between the true head direction from the tracking system α_{true} and the population decoded head direction α_{dec} (both shown in 2D):

$$\beta_{\text{dec}} = \alpha_{\text{dec}} - \alpha_{\text{true}}. \tag{6}$$

From the recorded position of the mouse, we also obtain the lateral and longitudinal offset to the visual cue Δx and Δy.

We then perform a linear regression

$$\beta_{\text{dec}}(t) = w \cdot \arctan\left(\frac{\Delta y(t)}{\Delta x(t)}\right) + b + \varepsilon(t), \tag{7}$$

where the slope w and intercept b are fitted parameters minimizing the squared error of the linear fit to the observed data points. ε is the residual. To account for autocorrelations in the time series data, we use stationary block bootstrapping (Politis & and, 1994) with an average block length of 2 s to estimate the standard errors of w and b. For the linear regression, outliers ($\beta_{\text{dec}} \geq 36°$) were removed, as such large errors likely arose from decoding artifacts (Suppl. Fig 12 for results without the outlier rejection).

Eq. 7 corresponds to Eq 5 where the slope is $w = -1$ and the intercept $b = -w \cdot \gamma_{\text{anchor}}$. Note that the linear regression fits the y-intercept, while the anchoring angle is the x-intercept.

A purely visual cue-based head direction signal would predict a slope of $w = -1$ (full parallax-error) and an x-intercept corresponding to the specific cue's anchoring angle γ_{anchor}.

We assume that each cue and each animal has a distinct anchoring angle. Therefore, the fit is performed separately for each mouse, as shown in Fig. 3. The parallax error can be observed and is statistically significant in all 6 recordings. However, the slope w has a magnitude lower than 1, indicating a lower parallax-induced error than a pure vision model. Furthermore, the relatively low R^2 values suggest that additional factors influence HD decoding errors. One important and well-known additional factor is AHV integration.

The need for AHV integration is particularly clear when the mouse does not see the cue. We therefore also investigated whether parallax remains when the cue is invisible. A lower parallax can be assumed because AHV integrates noise and more importantly, the cue angle (Θ_{cue}) can change when the mouse walks around while the cue is invisible. During these periods, the last seen parallax error is roughly maintained, reducing the slope in these periods. Fig. 3B indeed shows a tendency towards lower parallax error when the cue is behind the mouse (and can therefore be assumed invisible). The lower slope of invisible cue vs. visible cue is significant in 3 of the 6 mice (Supplementary Fig. 13 and 14) and can also be observed in the simulation which we introduce below (Fig. 4B).

Angular Head Velocity Integration Passively Attenuates Parallax Error

The observation that parallax error exists suggests that the HD system relies on simple visual anchoring. Naively, one might also conclude that an explicit correction mechanism has to exist, as the magnitude of the slope w is less than 1. However, this assumes pure visual landmark-based HD. Previous research has established that HD cells in the postsubiculum not only rely on vision but rather integrate angular head velocity from the vestibular system and proprioception and use visual cues only to anchor integration to avoid drift (Blair & Sharp, 1996; Goodridge et al., 1998; Knierim et al., 1995; Zugaro, Berthoz, & Wiener, 2001; Zugaro, Tabuchi, et al., 2001; Ocko et al., 2018; Page & Jeffery, 2018).

The fact that vision referencing happens at different positions while the animal is walking around might lead passively to an averaging out of parallax error: When the animal is on the right of the anchoring axis (Fig. 5), the error is negative, while it is positive on the left side, so, on average, the error equals out. While we do not show this here, the averaging effect is expected to be much stronger with multiple cues (Gaussier et al., 2019), so a complex position-dependent or learning-based parallax correction mechanism might not be required.

To test this and quantify this automatic attenuation of parallax error via position error averaging, we implemented a combined integrate-and-vision model (existing in the literature in various degrees of complexity, e.g., McNaughton et al. (1991, 2006); Page & Jeffery (2018); Bicanski & Burgess (2016)) where the estimated head direction α_{iv} is simply computed as a weighted sum of the vision-based and AHV-integrated estimates:

$$\alpha_{\text{iv}}(t) = \sigma \cdot \alpha_{\text{int}}(t) + (1-\sigma) \cdot \alpha_{\text{vis}}(t) \cdot v_{cue}(t), \tag{8}$$

where σ is a parameter determining the relative weighting of AHV integration and visual anchoring. $v_{cue}(t)$ is a binary variable indicating whether the cue is within the 180° visual field. The weighting $\sigma = 0.995$ minimizes the mean squared error between the α_{iv} and α_{dec}. The integrated estimate $\alpha_{\text{int}}(t)$ is recursively computed from AHV and the previous state of the integrate-and-vision model:

$$\alpha_{\text{int}}(t) = \alpha_{\text{iv}}(t-1) + \Delta\alpha(t), \tag{9}$$

where $\Delta\alpha(t)$ is the angular displacement derived from head tracking data, assuming noise-free integration. So, $\text{AHV}(t) = \frac{\Delta\alpha(t)}{\Delta t}$.

Ideally, this would be calculated using a Bayesian update. However, here, we use a fixed σ instead of making it dependent on the variance of α_{int} and α_{vis} because the variance of α_{int} in the neural system is not known and we use the AHV of the tracking system which is very precise. γ_{anchor} is set to 90° (i.e., north) in this model. Fig. 4A shows the fitted lines from 3 for comparison, and Fig. 4B shows that incorporating AHV integration is sufficient to reduce the parallax error. This indicates that parallax errors can indeed be attenuated passively through integration even without additional correction mechanisms. Note that the modeled slope w is quite sensitive to the weighting parameter σ, which we cannot estimate reliably. A larger σ leads to a lower weighting of the visual anchoring and therefore a lower slope. The model is also able to capture the difference in slope between cue visibility conditions. Data points where the simulated mouse is able to see the cue show a higher slope than the ones where the cue is invisible.

Inferring the Anchoring Angle from Parallax

The anchoring angle γ_{anchor} can be interpreted as the (allocentric) head direction the animal had when it anchored the cue. I.e., the HD system 'decided' that this particular cue has a certain angle offset to its current head direction. This means that at this particular angle, no parallax is expected. In Fig. 3, this corresponds to the x-intercept of the linear regression, which we can compute using the fitted slope and y-intercept:

$$\gamma_{\text{anchor}} = \frac{-b}{w}. \tag{10}$$

The computed anchoring angles per mouse can also be found in the legend of each plot in Fig. 3.

An alternative intuition for γ_{anchor} is the expected egocentric angle of the cue when the animal is at 0 head direction. In our case, it is the angle at which the HD system 'expects' the cue when the animal looks exactly eastward (towards the origin of the allocentric angle). What determines the anchoring angle is an interesting question that we do not address here. Presumably, the animal learned a mapping between the cue-specific bearing cell angle representation and the heading direction. We hypothesize that mechanistically, the anchoring

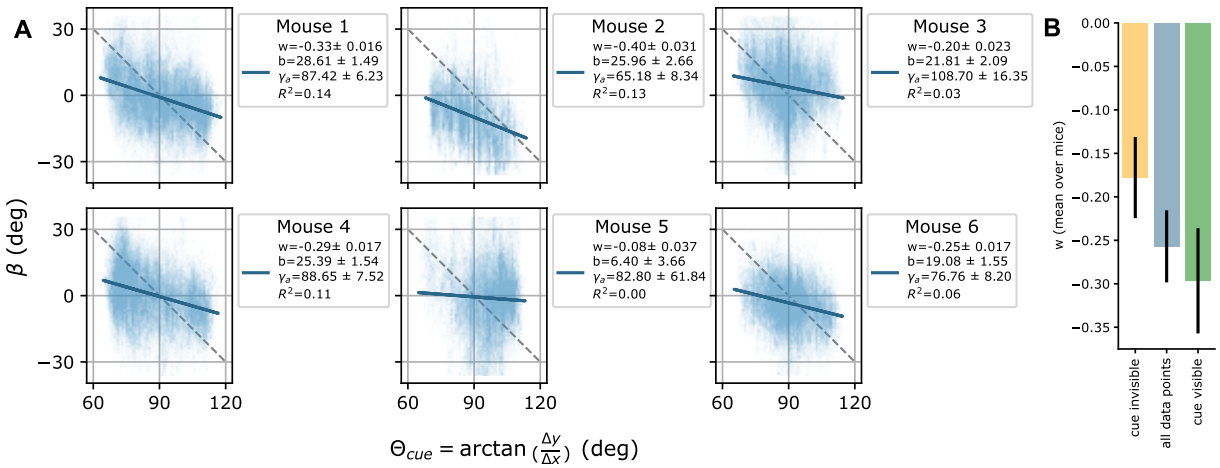

Figure 3: **Quantification of the parallax-induced error in head direction (HD) estimation across different recording sessions. (A):** Each panel shows the relationship between the allocentric angle of the vector from the animal to the cue $\theta_{\text{cue}} = \arctan\left(\frac{\Delta y(t)}{\Delta x(t)}\right)$ and the observed angular error β_{dec} as in Eq. 7. Individual data points are calculated from the decoded HD traces of the TH-2 dataset, lines indicate the fitted linear model. The consistent nonzero slopes confirm a parallax effect. Apart from mouse 5, all regressions have statistically significant slopes ($p << 0.001$), rejecting the null hypothesis of no systematic error. For further illustration of the parallax effect, see Suppl. Fig. 7-10. **(B)** shows the mean slopes depending on whether the cue is within the hypothetical 180° visual field of the mice. We observe a tendency towards a higher slope when the cue is visible.

angle may be the angle offset between cue-specific bearing cell ring(s) and the HD cell ring. For now, we also assume that γ_{anchor} is fixed over time (see next section for more analysis).

Fig. 5 (and Suppl. Fig. 15) explore whether the anchoring angle of the HD system can be inferred from the spatial distribution of parallax-induced errors.

To test this, we analyzed the recorded decoding error β across different animal trajectories and compared it to predictions from a naive anchoring model. The model assumes that if the HD system solely relies on visual anchoring without position-dependent corrections, the systematic bias β should vary predictably with spatial position. In Fig. 5A, the mean of the observed β_{dec} per position bin is color-coded, showing distinct spatial patterns of systematic error. Fig. 5B presents theoretical predictions based on the naive anchoring model, demonstrating that the rotation of the anchoring axis aligns with the fitted intercept from Fig. 3.

These results indicate that the anchoring angle can be inferred from spatially distributed parallax errors, providing a potential method for calculating it from neural recordings. Furthermore, this analysis supports the notion that HD anchoring occurs at a specific egocentric angle relative to visual landmarks.

Anchoring Angle is Approximately Conserved over Time and over Cue Switches

Using Eq. 10 to estimate the anchoring angle γ_{anchor}, we can now investigate how stable the anchoring angle, which we have assumed as constant for now, is. The data (Duszkiewicz et al., 2024) contains 90° cue switches between trials. Since the decoded HD follows these cue switches, the HD system seems to treat the two cues as a single reference, i.e., maintaining the same anchoring angle without re-anchoring. Fig. 6A indeed shows that γ_{anchor} there is no significant change between the two cue conditions, indicating that it remains stable.

We also investigated if γ_{anchor} drifts over time. Fig. 6B shows that the estimated γ_{anchor} is not significantly different in the first half of the data than in the second half of the data.

Anchoring angles seem to be distributed around the center (Fig. 6). A distribution within less than 360° is expected because the HD system can likely only anchor to a cue if it is in the field of vision, and the platform only allows a small movement range. However, at least in this small sample, most anchoring angles are within only about 40°, corresponding to the size of the platform. This could indicate preferred anchoring in an area of increased visual acuity (van Beest et al., 2021) (i.e. when the animal is looking directly at it). These observations and hypotheses should be investigated further in larger environments. Furthermore, to improve the precision of the anchoring angle estimate it seems necessary to use longer recordings or record more neurons.

Software

Code was written in Python 3.12 using numpy, matplotlib, and scipy for analysis and visualization. Fits were performed using the scipy.stats.linregress function, bootstrapping using the arch package and MSE minimization for σ using the optuna package.

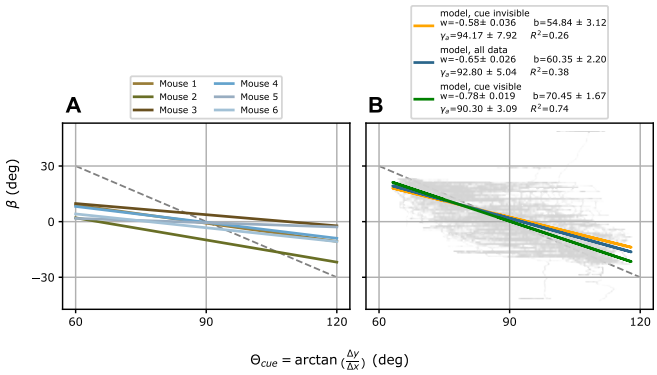

Figure 4: **AHV integration attenuates parallax-induced errors in head direction (HD) estimation.** (**A**) Fitted slopes w (according to Eq 7) of the parallax effect for all experimental recording sessions as already shown in Fig. 3. Slopes show a consistent parallax error, but the error is smaller than expected from a purely vision-based model ($w = -1$, shown in the background). (**B**) The combined integrate-and-vision model demonstrates partial error attenuation, closely matching the slope of the experimental data. Gray points from simulated data using the recorded trajectory of mouse 1. The three regression lines correspond to all data (blue), only time bins where the cue is assumed invisible (180° field of view, yellow), or only time points where the cue is visible (green).

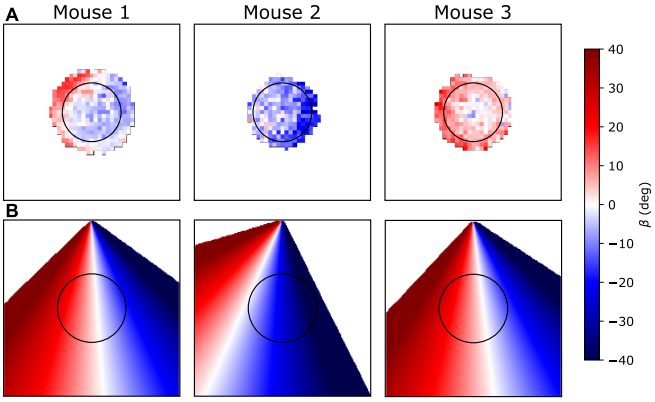

Figure 5: **Estimating the anchoring angle γ_{anchor} based on parallax effects.** (**A**) Heatmaps of the animal during three different recording sessions, color-coded by the observed angular error β_{dec} of the neural data at each location. (**B**) Predictions of the spatial distribution of β from the model fitted via linear regression, as shown in Fig. 3. The heatmaps show the systematic parallax error, corresponding to the errors observed in the data plotted in panel A (each A-B pair corresponds to one animal). These findings suggest that the anchoring angle can be inferred from spatially distributed parallax errors. Mice 4-6 in Suppl. Fig. 15.

Discussion

Relevance

To our knowledge, this is the first systematic documentation of a parallax error in mammalian HD cells. While models have predicted that simple visual anchoring could produce parallax errors (Bicanski & Burgess, 2016), direct neural evidence for such effects has been limited. Our findings provide empirical support for this prediction and suggest that these errors persist despite AHV integration if only a single cue is available. One reason for the limited evidence of parallax error in the HD system may be that few datasets that use a single cue are publicly available. Even in such datasets, additional environmental cues (e.g., shadows, visible corners or borders, odors, etc.) could be used to compensate for the error.

Our findings indicate that, at least in environments with a single cue, the HD system relies on simple visual anchoring, leading to systematic parallax-induced errors. AHV integration appears to passively reduce these errors by averaging across different anchoring positions and is likely to reduce them further if multiple cues are available. However, in more complex settings, we cannot exclude the possibility that positional signals from the entorhinal cortex or learned compensatory mechanisms might further reduce or eliminate parallax effects. For instance, such a compensatory mechanism could estimate the relative position of cues from visual input to calculate a correction.

Egocentric visual cue anchoring is a fast and computationally efficient mechanism for stabilizing the HD signal, particularly in familiar environments and when distal cues are available. For this simple strategy, only the retinal location of a cue and the eye angle need to be known to compute a head direction estimate. Efficient and robust algorithms for HD estimation are not just relevant for computational neuroscience but also have implications for neuromorphic robotics, where simple computations are important for energy efficiency (Arleo & Gerstner, 2000; Kreiser et al., 2020; Renner et al., 2022). Navigation and SLAM models can be made more efficient if they can assume a stable and robust head direction that does not rely on positional information.

Our results might also open the door for a potential novel paradigm for estimating the anchoring properties of HD cells based on parallax errors. By mapping spatial distributions of decoding errors, we inferred the egocentric angle at which the HD system anchors, suggesting that the anchoring angle is a measurable property of the network. This approach may provide insights into how HD cells calibrate to different environmental conditions and sensory inputs and could elucidate if and how anchoring is learned.

Limitations of this Study

It is crucial to validate our findings on additional datasets. While the parallax error appears consistent across all recording sessions and cue conditions, the reliance on a single dataset limits generalizability. Furthermore, although our results suggest that the HD system primarily integrates AHV with visual anchoring rather than performing complex positional corrections, we cannot rule out the possibility that additional compensatory mechanisms might emerge in larger en-

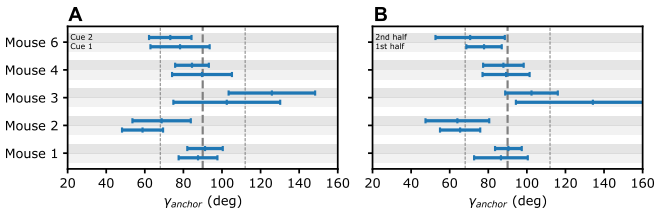

Figure 6: **Anchoring angle (γ_{anchor}) is unique for each session and is conserved over cue switches**. (**A**) Estimated γ_{anchor} for 5 out of 6 sessions and the two cue conditions: Unrotated cue in dark grey and $\pm 90^\circ$ rotated cue in light grey. Mouse 5, with the fewest amount of recorded HD neurons, was excluded due to small slope and large errors (compare Fig. 3). γ_{anchor} varies only slightly between cue conditions (corrected for the 90° rotation of the head direction). Error bars show standard errors of the intercept of the linear regression obtained by block bootstrapping. (**B**) Estimated γ_{anchor} over time: First half of the data in dark grey and second half in light grey. γ_{anchor} does not vary significantly over time.

vironments or over longer timescales. Part of the slope reduction we observed might also be due to unintended cues (e.g., odors) or existing correction mechanisms, which were only partially employed as the cue was assumed to be further away or because the system was unable to estimate the position of the cue correctly due to the environmental conditions. It was, for instance, observed that bright cues can be perceived as (distal) celestial bodies in insects (Giraldo et al., 2018; Nguyen et al., 2022). This could mean that dimmer cues might alter the strength of parallax effects, requiring further investigation. Furthermore, the cue here is outside of the platform and, therefore, not reachable by the mouse, which could also lead to it being classified as a distal cue (Cressant et al., 1997).

The weighting parameter σ between vision and integration should be interpreted cautiously. It underestimates the contribution of vision because the cue has a certain width and is not a point source and because our model assumes noise-free integration. The point of this simple model was merely to show that AHV integration passively attenuates parallax-induced errors.

In general, the relatively low explained variance by the simple model might be due to many possible factors, such as decoding errors (due to a limited amount of recorded HD cells), limited precision of AHV and AHV integration (tracking and neural), and limited visual acuity. We should bear in mind that the decoding error β is a relatively small quantity compared to the decoded angle α_{dec} and the tracking HD α_{true}.

While Δy is part of our equations, we did not separately investigate the distance-dependency of the parallax error because the platform was at a distance where parallax errors were relatively stable (Fig. 2), and the lateral translation effect and noise were more pronounced than distance dependency. Future work could investigate distance dependency in larger arenas and closer cues.

Finally, it is important to acknowledge that while simple visual anchoring explains many of the observed patterns in our data, it does not fully account for the complexity of HD computation in natural settings. The HD network integrates multiple sensory modalities beyond vision and vestibular input, including auditory, olfactory, and proprioceptive information, to maintain a robust and flexible representation of head direction (Stackman & Taube, 1997, 1998; Fortenberry et al., 2012). Future work should aim to develop computational models that capture this multisensory integration in diverse environments and test how the weighting of these cues adapts to changing sensory contexts.

A more comprehensive model of visual anchoring in the head-direction (HD) system would need to integrate multiple sensory and contextual factors beyond simple cue anchoring. Such a model should incorporate the stability, distance, familiarity, and salience of visual cues, all of which are known to influence the reliability and weighting of external landmarks. For instance, stable and distal cues have been shown to exert stronger control over the HD network compared to nearby or dynamic landmarks (Blair & Sharp, 1996; Julian et al., 2018). Familiarity with specific visual landmarks also plays a critical role, with well-learned cues dominating the network's response in familiar environments (Goodridge et al., 1998). Although our data did not allow us to construct such a complex, integrative model, and this was not the goal of our study, our findings emphasize the need for future research to explore how these factors dynamically influence cue weighting. Bayesian (Cheng et al., 2007) or learning-based (Fortenberry et al., 2012) frameworks for multisensory integration offer a promising approach for modeling this process, where the contribution of each cue could be weighted based on its reliability and relevance in a given context. This would explain the higher weighting of static cues and the distance-dependency of cue weighting observed by Taube (1995); Blair & Sharp (1996); Zugaro, Tabuchi, et al. (2001); Julian et al. (2018) because close cues have a larger parallax-induced variance (high variance leads to lower weighting).

Further Research

Several aspects of this study suggest avenues for future research. Modeling data from larger environments with multiple cues (Stackman & Taube, 1998; Blair & Sharp, 1996; Julian et al., 2018) would help test how the HD system integrates visual landmarks and integrates them with vestibular inputs. It should also be taken into account that environmental geometry plays a role in anchoring the HD signal, as suggested by work on spatial orientation in disoriented navigators (Julian et al., 2015, 2018).

It might also be interesting to investigate if parallax is present in other brain areas (see Fig. 1 for connectivity in the HD system). As LMN receives visual-corrected input from PoSub (Yoder et al., 2015; Stackman & Taube, 1998), there is reason to believe that it may show such an error. If it is true that parallax correction is not necessary, HD-sensitive cells

downstream in the entorhinal cortex should also be affected, even if they would have positional information to correct for it.

An open question is whether the anchoring angle γ_{anchor} is stable or dynamic and whether it is learned for each cue or computed based on unique cue features. A feature-based computation would allow for faster and more robust adaptation to new environments, but there is also evidence for learning in the HD system (Goodridge et al., 1998; Yoder et al., 2015) and many models employ learning for HD computation (Fortenberry et al., 2012; Page & Jeffery, 2018; Ocko et al., 2018). The proposed method for estimating γ_{anchor} could help resolve this question in future research but longer recordings or more recorded HD neurons are needed to improve the precision of the estimate.

Conclusion

Our findings provide evidence that the HD system exhibits systematic parallax errors when relying on a single visual cue, suggesting that it primarily employs simple egocentric anchoring rather than explicit position-dependent corrections. However, AHV integration passively attenuates these errors, and in natural environments, multiple cues likely further reduce or eliminate them through averaging. This highlights a fundamental trade-off in neural coding between computational simplicity and positional accuracy.

While our results suggest that the HD system does not require complex correction mechanisms under these conditions, future research should explore whether learned adjustments or multimodal integration refine this process over time. Our proposed method of estimating the anchoring angle from spatially distributed parallax errors provides a potential tool that could help reveal how the HD system anchors. Understanding these principles has implications beyond neuroscience, informing the development of robust, bio-inspired navigation systems.

Acknowledgements

For this work, the data from Duszkiewicz et al. (2024) was used, and we thank the authors for making this data available. The data can be found here: 10.6084/m9.figshare.24921252). We especially thank Adrian Duszkiewicz for answering our questions regarding the dataset, and Johannes Leugering and Paxon Frady for their feedback. OpenAI ChatGPT was used to optimize and document code and to support writing.

This research is funded by VolkswagenStiftung [CLAM 9C854].

References

Alexander, A. S., Carstensen, L. C., Hinman, J. R., Raudies, F., Chapman, G. W., & Hasselmo, M. E. (2020). Egocentric boundary vector tuning of the retrosplenial cortex. *Science advances*, *6*(8), eaaz2322.

Arleo, A., & Gerstner, W. (2000). Modeling rodent head-direction cells and place cells for spatial learning in biomimetic robotics. *From Animals to Animats*, *6*, 236–245.

Bicanski, A., & Burgess, N. (2016). Environmental anchoring of head direction in a computational model of retrosplenial cortex. *Journal of Neuroscience*, *36*(46), 11601–11618.

Blair, H. T., & Sharp, P. E. (1996). Visual and vestibular influences on head-direction cells in the anterior thalamus of the rat. *Behavioral neuroscience*, *110*(4), 643.

Butler, W. N., Smith, K. S., van der Meer, M. A., & Taube, J. S. (2017). The head-direction signal plays a functional role as a neural compass during navigation. *Current Biology*, *27*(9), 1259–1267.

Chaudhuri, R., Gerçek, B., Pandey, B., Peyrache, A., & Fiete, I. (2019, September). The intrinsic attractor manifold and population dynamics of a canonical cognitive circuit across waking and sleep. *Nature Neuroscience*, *22*(9), 1512–1520. doi: 10.1038/s41593-019-0460-x

Cheng, K., Shettleworth, S. J., Huttenlocher, J., & Rieser, J. J. (2007). Bayesian integration of spatial information. *Psychological bulletin*, *133*(4), 625.

Cressant, A., Muller, R. U., & Poucet, B. (1997). Failure of centrally placed objects to control the firing fields of hippocampal place cells. *Journal of Neuroscience*, *17*(7), 2531–2542.

Duszkiewicz, A. J., Orhan, P., Skromne Carrasco, S., Brown, E. H., Owczarek, E., Vite, G. R., . . . Peyrache, A. (2024, April). Local origin of excitatory–inhibitory tuning equivalence in a cortical network. *Nature Neuroscience*, *27*(4), 782–792. doi: 10.1038/s41593-024-01588-5

Fortenberry, B., Gorchetchnikov, A., & Grossberg, S. (2012). Learned integration of visual, vestibular, and motor cues in multiple brain regions computes head direction during visually guided navigation. *Hippocampus*, *22*(12), 2219–2237.

Gaussier, P., Banquet, J. P., Cuperlier, N., Quoy, M., Aubin, L., Jacob, P.-Y., . . . Poucet, B. (2019). Merging information in the entorhinal cortex: what can we learn from robotics experiments and modeling? *Journal of Experimental Biology*, *222*(Suppl_1), jeb186932.

Giocomo, L. M., Stensola, T., Bonnevie, T., Van Cauter, T., Moser, M.-B., & Moser, E. I. (2014). Topography of head direction cells in medial entorhinal cortex. *Current Biology*, *24*(3), 252–262.

Giraldo, Y. M., Leitch, K. J., Ros, I. G., Warren, T. L., Weir, P. T., & Dickinson, M. H. (2018). Sun navigation requires compass neurons in drosophila. *Current Biology*, *28*(17), 2845–2852.

Goodridge, J. P., Dudchenko, P. A., Worboys, K. A., Golob, E. J., & Taube, J. S. (1998). Cue control and head direction cells. *Behavioral neuroscience*, *112*(4), 749.

Hulse, B. K., & Jayaraman, V. (2020). Mechanisms underlying the neural computation of head direction. *Annual review of neuroscience*, *43*(1), 31–54.

Julian, J. B., Keinath, A. T., Marchette, S. A., & Epstein, R. A. (2018). The neurocognitive basis of spatial reorientation. *Current Biology*, *28*(17), R1059–R1073.

Julian, J. B., Keinath, A. T., Muzzio, I. A., & Epstein, R. A. (2015). Place recognition and heading retrieval are mediated by dissociable cognitive systems in mice. *Proceedings of the National Academy of Sciences*, *112*(20), 6503–6508.

Knierim, J. J., & Hamilton, D. A. (2011). Framing spatial cognition: neural representations of proximal and distal frames of reference and their roles in navigation. *Physiological reviews*, *91*(4), 1245–1279.

Knierim, J. J., Kudrimoti, H. S., & McNaughton, B. L. (1995). Place cells, head direction cells, and the learning of landmark stability. *Journal of Neuroscience*, *15*(3), 1648–1659.

Kreiser, R., Renner, A., Leite, V. R., Serhan, B., Bartolozzi, C., Glover, A., & Sandamirskaya, Y. (2020). An on-chip spiking neural network for estimation of the head pose of the icub robot. *Frontiers in Neuroscience*, *14*, 551.

McNaughton, B. L., Battaglia, F. P., Jensen, O., Moser, E. I., & Moser, M.-B. (2006, August). Path integration and the neural basis of the 'cognitive map'. *Nature Reviews Neuroscience*, *7*(8), 663–678. doi: 10.1038/nrn1932

McNaughton, B. L., Chen, L., & Markus, E. (1991). "dead reckoning," landmark learning, and the sense of direction: a neurophysiological and computational hypothesis. *Journal of Cognitive Neuroscience*, *3*(2), 190–202.

Nguyen, T. A. T., Beetz, M. J., Merlin, C., Pfeiffer, K., & El Jundi, B. (2022). Weighting of celestial and terrestrial cues in the monarch butterfly central complex. *Frontiers in Neural Circuits*, *16*, 862279.

Ocko, S. A., Hardcastle, K., Giocomo, L. M., & Ganguli, S. (2018). Emergent elasticity in the neural code for space. *Proceedings of the National Academy of Sciences*, *115*(50), E11798–E11806.

Page, H. J., & Jeffery, K. J. (2018). Landmark-based updating of the head direction system by retrosplenial cortex: a computational model. *Frontiers in Cellular Neuroscience*, *12*, 191.

Politis, D. N., & and, J. P. R. (1994). The stationary bootstrap. *Journal of the American Statistical Association*, *89*(428), 1303–1313. Retrieved from `https://doi.org/10.1080/01621459.1994.10476870` doi: 10.1080/01621459.1994.10476870

Rank, J. (1984). Head-direction cells in the deep layers of dorsal presubiculum of freely moving rats. In *Soc. neuroscience abstr.* (Vol. 10, p. 599).

Redish, A. D., Elga, A. N., & Touretzky, D. S. (1996). A coupled attractor model of the rodent head direction system. *Network: computation in neural systems*, *7*(4), 671.

Renner, A., Supic, L., Danielescu, A., Indiveri, G., Frady, E. P., Sommer, F. T., & Sandamirskaya, Y. (2022). Visual odometry with neuromorphic resonator networks. *arXiv preprint arXiv:2209.02000*.

Skaggs, W., Knierim, J., Kudrimoti, H., & McNaughton, B. (1994). A model of the neural basis of the rat's sense of direction. *Advances in neural information processing systems*, *7*.

Stackman, R. W., & Taube, J. S. (1997). Firing properties of head direction cells in the rat anterior thalamic nucleus: dependence on vestibular input. *Journal of Neuroscience*, *17*(11), 4349–4358.

Stackman, R. W., & Taube, J. S. (1998). Firing properties of rat lateral mammillary single units: head direction, head pitch, and angular head velocity. *Journal of Neuroscience*, *18*(21), 9020–9037.

Stratton, P., Wyeth, G., & Wiles, J. (2010). Calibration of the head direction network: a role for symmetric angular head velocity cells. *Journal of computational neuroscience*, *28*, 527–538.

Taube, J. S. (1995). Head direction cells recorded in the anterior thalamic nuclei of freely moving rats. *Journal of Neuroscience*, *15*(1), 70–86.

Taube, J. S. (2007, July). The Head Direction Signal: Origins and Sensory-Motor Integration. *Annual Review of Neuroscience*, *30*(Volume 30, 2007), 181–207. doi: 10.1146/annurev.neuro.29.051605.112854

Taube, J. S., Muller, R. U., & Ranck, J. B. (1990a, February). Head-direction cells recorded from the postsubiculum in freely moving rats. I. Description and quantitative analysis. *The Journal of Neuroscience: The Official Journal of the Society for Neuroscience*, *10*(2), 420–435. doi: 10.1523/JNEUROSCI.10-02-00420.1990

Taube, J. S., Muller, R. U., & Ranck, J. B. (1990b). Head-direction cells recorded from the postsubiculum in freely moving rats. ii. effects of environmental manipulations. *Journal of Neuroscience*, *10*(2), 436–447.

van Beest, E. H., Mukherjee, S., Kirchberger, L., Schnabel, U. H., van der Togt, C., Teeuwen, R. R., ... others (2021). Mouse visual cortex contains a region of enhanced spatial resolution. *Nature communications*, *12*(1), 4029.

Wilton, L., Baird, A. L., Muir, J. L., Honey, R. C., & Aggleton, J. P. (2001). Loss of the thalamic nuclei for" head direction" impairs performance on spatial memory tasks in rats. *Behavioral neuroscience*, *115*(4), 861.

Winter, S. S., Clark, B. J., & Taube, J. S. (2015). Disruption of the head direction cell network impairs the parahippocampal grid cell signal. *Science*, *347*(6224), 870–874.

Yoder, R. M., Peck, J. R., & Taube, J. S. (2015). Visual landmark information gains control of the head direction signal at the lateral mammillary nuclei. *Journal of Neuroscience*, *35*(4), 1354–1367.

Zhang, K. (1996). Representation of spatial orientation by the intrinsic dynamics of the head-direction cell ensemble: a theory. *Journal of Neuroscience*, *16*(6), 2112–2126.

Zhang, K., Ginzburg, I., McNaughton, B. L., & Sejnowski, T. J. (1998). Interpreting neuronal population activity by reconstruction: unified framework with application to hippocampal place cells. *Journal of neurophysiology*, *79*(2), 1017–1044.

Zugaro, M. B., Berthoz, A., & Wiener, S. I. (2001, July). Background, But Not Foreground, Spatial Cues Are Taken

as References for Head Direction Responses by Rat Anterodorsal Thalamus Neurons. *The Journal of Neuroscience*, *21*(14), RC154-RC154. doi: 10.1523/JNEUROSCI.21-14-j0001.2001

Zugaro, M. B., Tabuchi, E., Fouquier, C., Berthoz, A., & Wiener, S. I. (2001). Active locomotion increases peak firing rates of anterodorsal thalamic head direction cells. *Journal of neurophysiology*, *86*(2), 692–702.

Supplementary Figures

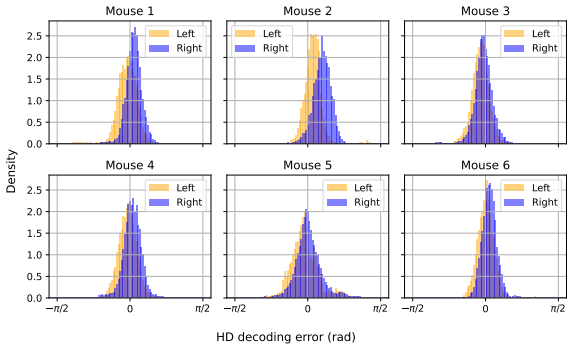

Figure 7: **Decoding error histograms by platform region (only cue 1, left - right).** Histograms of decoding errors for cue 1 trials when the mouse is in the right (blue) or left (yellow) third of the platform. The cue is at the top of the arena. As expected from the parallax effect, the error distribution right of the cue is shifted to the right while the errors left of the cue are shifted to the left.

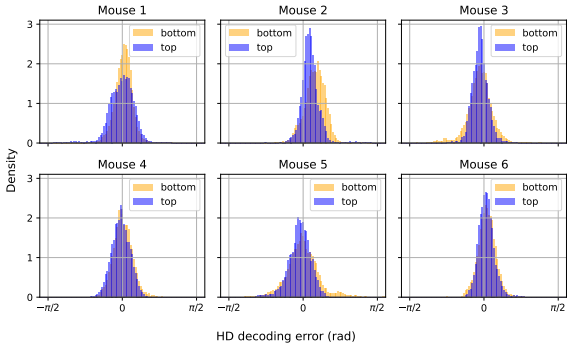

Figure 8: **Decoding error histograms by platform region (only cue 1, bottom - top).** Histograms of decoding errors when the mouse is in the near (blue, top third) or far (yellow, bottom third) region relative to the cue. As expected, only a minor parallax-induced shift is observed, since the mouse only moves toward or away from the cue. The shift observed in mouse 2 reflects the large anchoring angle, as visualized in Fig. 5.

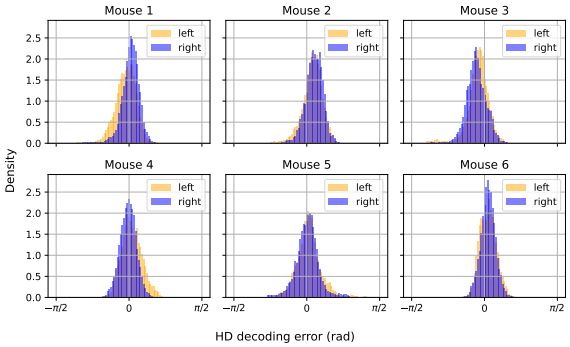

Figure 9: **Decoding error histograms by platform region (only cue 2, left - right).** Histograms of decoding errors for the rotated cue trials, when the mouse is either on the left (yellow) or right (blue) side of the platform. The rotated cues are located to the right of the platform for mice 1-3 and to the left of the platform for mice 4-6. As expected, we do not observe strong parallax effects in this setting, as the blue and yellow histograms correspond to points on the platform where the mouse is either near or far away from the cue. Note that for the analysis in the rest of the paper, we used a cue-centric coordinate system to align both cue conditions.

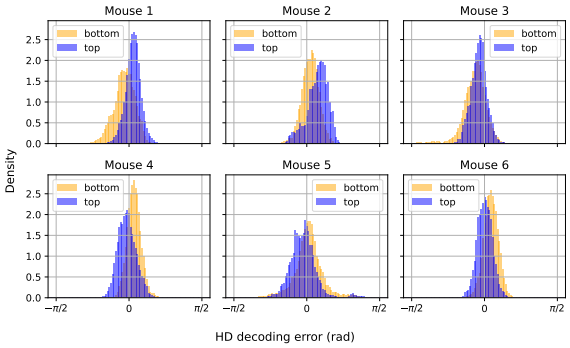

Figure 10: **Decoding error histograms by platform region (only cue 2, bottom - top).** Histograms of decoding errors for the rotated cue trials, when the mouse is either on the bottom (lower third of the platform, yellow) or top (upper third of the platform, blue) side of the platform. The rotated cues are located to the right of the platform for mice 1-3 and to the left of the platform for mice 4-6. Therefore, the top-bottom split of the data corresponds to horizontal offsets to the cue and we therefore see, as expected, the parallax effect in the data. As mice 4-6 see the cue rotating in the opposite direction, we also see, as expected, that the shift between the yellow and blue distribution is now exactly flipped, compared to the sessions of mice 1-3. Note that for the analysis in the rest of the paper, we used a cue-centric coordinate system to align both cue conditions.

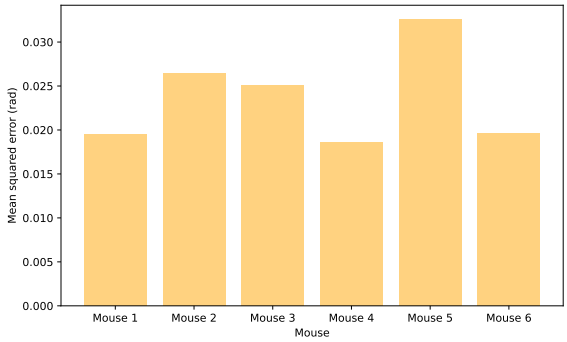

Figure 11: **Mean decoding error per session.** Bars show the root mean squared error between the tracked and decoded head direction. Switch periods and other rejected periods due to tracking errors are excluded from this data. The error correlates with the number of neurons available for decoding (see methods).

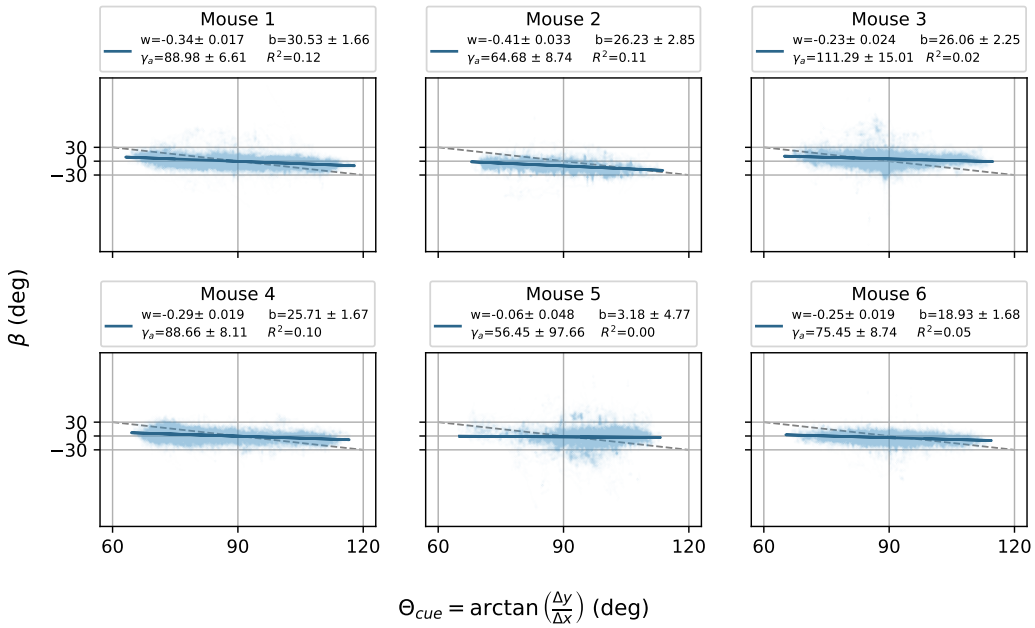

Figure 12: **Parallax analysis without outlier threshold.** Same analysis and presentation as presented in Fig. 3, but without outlier exclusion of very large decoding errors, as a control. Data rejection based on other factors than the decoding error was still performed. The outlier rejection does not qualitatively alter the results presented in the paper.

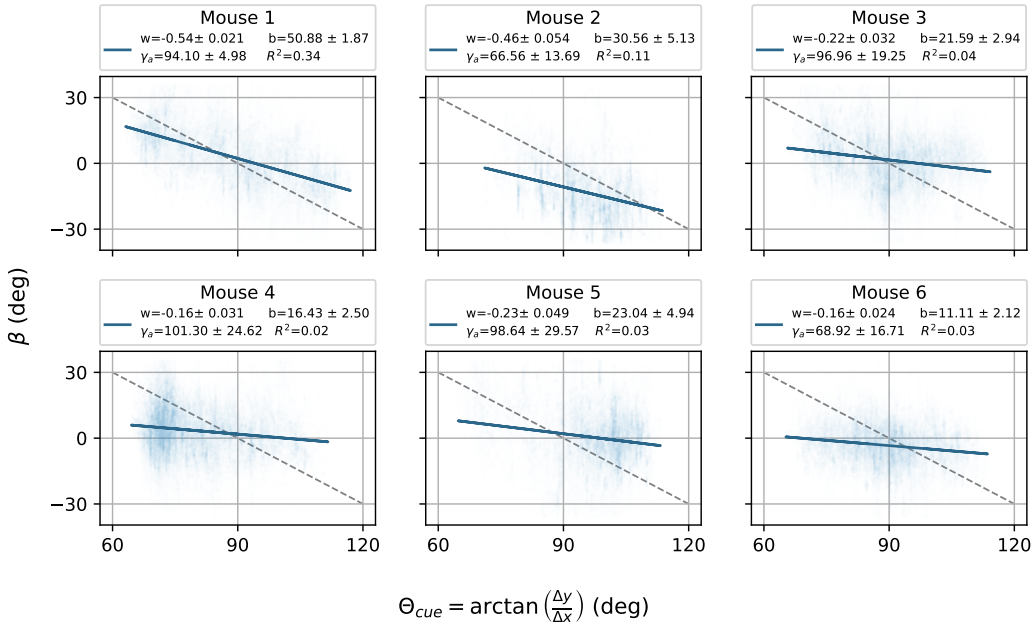

Figure 13: **Parallax when the cue is in front of the animal.** Same analysis as in Fig. 3, but only using data when the cue is in front of the animal and presumably visible, based on a visual field of 180° ($\pm 90^\circ$ around the current head direction).

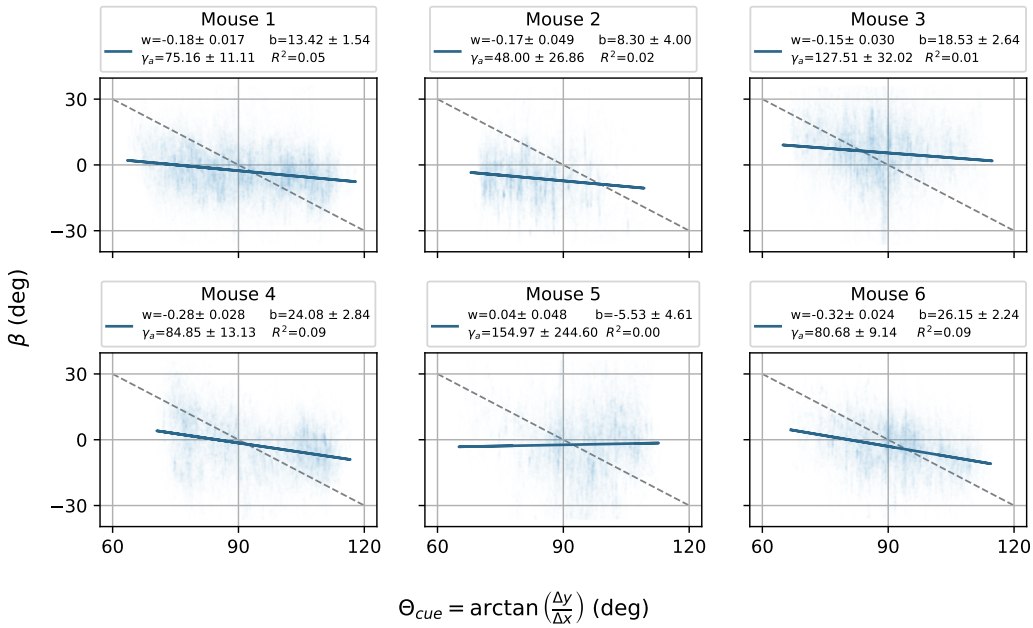

Figure 14: **Parallax when the cue is behind the animal.** Same analysis as in Fig. 3, but only using data when the cue is behind the animal and presumably invisible, based on a visual field of 180° ($\pm 90^\circ$ around the current head direction).

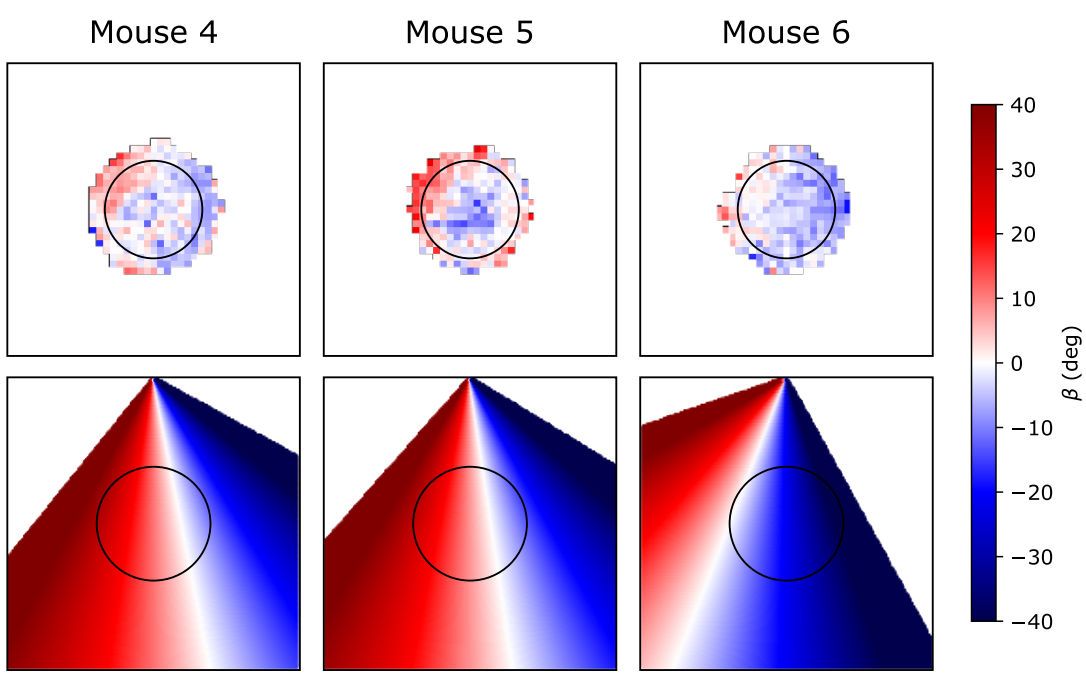

Figure 15: **Heatmap of measured parallax across space.** Same as Fig. 5, but for mice 4-6.

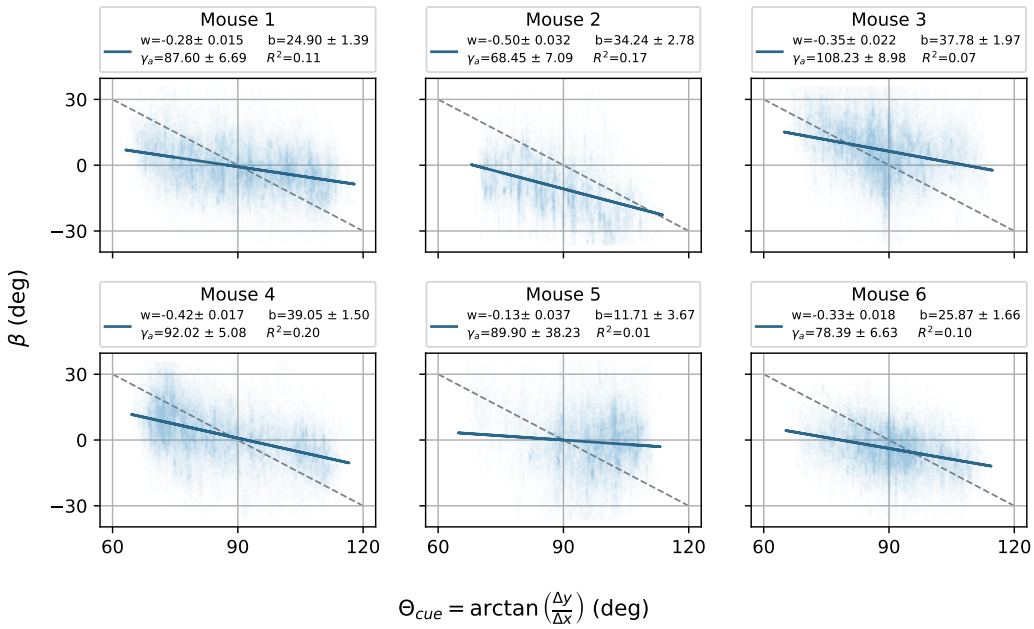

Figure 16: **Parallax using only center position tuning curves.** Same analysis as in Fig. 3, but using a different way of computing the tuning curves. This serves as a control that the anchoring angle is not affected by a position bias in the calibration phase from which we compute the tuning curves for the decoding. For this figure, we repeated the complete analysis pipeline while restricting the tuning curve estimations to data where the mouse is central on the platform (± 5 cm horizontal offset from the cue) ensuring only minor parallax. This does not change the anchoring angles meaningfully (compare anchoring angles to the ones in Fig. 3).